Recycled carbon fiber potential for reuse in carbon fiber/PA6 composite parts

Louis Jeantet, Arnaud Regazzi, Didier Perrin, Monica Francesca Pucci, Stéphane Corn, Jean-Christophe Quantin, Patrick Ienny

Recycled carbon fiber potential for reuse in carbon fiber/PA6 composite parts

Louis Jeantet[a,b,*], Arnaud Regazzi[b,*], Didier Perrin[c], Monica Francesca Pucci[b], Stéphane Corn[b], Jean-Christophe Quantin[b], Patrick Ienny[b]

[a]*Segula Technologies, 19 rue d'Arras, Nanterre, 92000, France*
[b]*LMGC, IMT Mines Ales, Univ Montpellier, CNRS, Ales, France*
[c]*Polymers Composites and Hybrids (PCH), IMT Mines Ales, Ales, France*

Abstract

Pyrolysis reclaiming is the most promising process to treat high volumes of composite waste with an advantageous carbon footprint. This paper aims to compare pyrolysis reclaimed carbon fibers (RCF) to virgin sized fibers (VF) and de-sized fibers (VFT) in their capability to bond to a polyamide 6 matrix. Micromechanical tensile testing of single fiber samples of the three fiber types was conducted. A minor reduction in tensile strength and an unchanged elastic modulus of the RCF compared to VF was observed. Scanning electron microscopy and atomic force microscopy scans were used to evaluate the morphology of the fibers. To evaluate the surface energy of the fibers, tensiometric testing was conducted. RCF showed a better adhesion capability compared to VFT through higher total surface energy. Moreover, X-ray spectrophotometry scans highlighted a higher proportion of functional groups at the RCF surface compared to VFT. Finally, pull-out tests underlined a decrease of the interfacial shear strength of RCF and VFT by 35 % compared to VF. Overall, this study's results further the understanding of the impact of the pyrolysis reclaiming process on RCF mechanical and adhesion properties.

Keywords: A. Carbon fibre, B. Fibre/matrix bond, D. Surface analysis, E. Recycling

*Corresponding authors
Email addresses: louis.jeantet@segula.fr (Louis Jeantet), arnaud.regazzi@mines-ales.fr (Arnaud Regazzi)

1. Introduction

Carbon fiber reinforced polymer (CFRP) composites are increasingly used in high performance industrial applications due to their extremely favorable strength to weight ratio. In particular, they have become the main materials used in aircraft manufacturing in recent years [1, 2]. Their use is also prevalent in automotive parts where their lightweight, high strength, excellent toughness, adequate chemical resistance, and thermal stability are highly useful [3]. The prevalence of those composite parts has created a need for a more sustainable production and a controlled life cycle. The demand for CFRP has increased from 100 kt in 2015 to 182 kt in 2021 and is estimated to reach 285 kt in 2025 [4]. A global production matching this exponential growth in CFRP demand would not be sustainable, especially since the production of virgin carbon fiber is a high emissions and high energy consumption process. Hence, there are both a sustainability and an economic incentive to reclaim and reuse carbon fibers (CF) from composite waste [5, 6]. However, composite waste recycling is a complex endeavor due to the intricate microstructure of these multiphasic materials [7, 8].

The most promising valorization methods consist in reclaiming CF after their separation from the matrix by means of chemical dissolution, exposition to high temperatures. Mechanical recycling is a mean of valorization of CFRP without separation of matrix from fibers. It is easier to implement, has lower CO_2 emissions and lower energy demands (respectively 1.77 kg CO_2eq./kg CFRP and 0.69 MJ/kg CFRP when the coarse fraction is incinerated[6]). However the recyled CFRP produced from this recycling method has poor mechanical performance making it inadequate for reuse in structural parts [9]. Fluidised bed and chemical recycling processes offer excellent preservation of fibre mechanical properties, most limit the amount of polymer residues, and have reasonable CO_2 emissions (1.5 kg CO_2eq./kg CFRP [6]). Yet, when taking into account the energy required for the production and processing of the solvents required in the chemical recycling, it results in a higher energy demand than fluidised bed (respectively 38 instead of 10 MJ/kg CFRP [6]). These RCF reclaiming methods are also difficult to apply to an industrial scale and the treatment of very high volumes of CFRP waste is not possible for the time being. Overall, to this day, the pyrolysis process turns out to be the most useful method for reclaiming CF from thermoset composites at an industrial scale [10]. It enables the treatment of very high volumes of CFRP waste (up to several tons per day). Although it is energy intensive, the

CO_2 emissions and energy demands (respectively 2.9 kg CO_2eq./kg CFRP and 37 MJ/kg CFRP [6]) are still advantageous compared to the production of virgin VF (respectively 25 kg CO_2eq./kg CFRP and between 198 and 595 MJ/kg CFRP [6]). The re-use of reclaimed CF (RCF) is nevertheless limited to short fiber composites since the entangled CF reclaimed by the pyrolysis are, for the time being, not reusable to produce new fabrics and thus new infused thermoset composites. Nevertheless, short CF can be used to produce structural parts in fused filament fabrication (FFF), a process that is well suited for the reuse of short RCF.

A major issue concerning RCF is the alteration of the fiber surface properties caused by the reclaiming process, leading to worsened cohesion between RCF and the matrix and thus, poor mechanical performance of the composite parts [11, 12]. The polymeric sizing used as a coating for the CF is mostly eliminated during the pyrolysis process. Yet, this sizing is a prime contributor to the interfacial strength. Thus, a surface treatment able to restore the interfacial strength between the CF and the polymer matrix might be necessary. Various surface modification approaches have been developed, such as physical, chemical oxidation [13, 14] and electrochemical treatment [15, 16].

Cold plasma physical treatment is also a promising option to restore surface roughness and chemical activity, and to promote cohesion of the CF to the polymer matrix. Its ability to increase the wettability of carbon fibers and the interfacial shear strength (IFSS) of CFRP using treated RCF has been demonstrated [17, 18, 19]. The combined efficiency and low environmental impact of this surface treatment make it perfectly suited to enhance the mechanical properties of CFRP using reclaimed CF through the functionalization of their surface.

This study aims to evaluate the factors that impact the interfacial properties of the pyrolysis RCF and in particular its ability to bond to a technical polymer matrix (i.e. polyamide 6). In the context of reusing reclaimed short carbon fiber with a thermoplastic matrix, polyamide 6 has great potential. Its mechanical properties as well as its processability allow for the production of high performance CFRP thermoplastic parts. The modifications of the wettability and chemistry of fibers surfaces by the reclaiming process were evaluated respectively via single fiber contact angle measurements and X-ray photoelectron spectrometry (XPS). The CF's surface morphology was also characterized via scanning electron microscopy (SEM) and atomic force microscopy (AFM). For the latter, the data collected were used to compute

roughness values. Finally, information on the fiber/matrix interaction in relation to CF adhesion properties was derived from IFSS measurements through microdroplet debonding tests.

2. Experimental

2.1. Materials

The thermoplastic matrix selected for the preparation of composites is Technyl C206F Natural, a commercially available polyamide 6 (PA6) produced by Solvay (Brussels, Belgium). Sized virgin fibers of different origins, obtained from spools of pure carbon fibers with a PA6 sizing and cut to a length of 20 mm, were supplied by Procotex (Mouscron, Belgium). Reclaimed carbon fibers were purchased from ELG Carbon Fiber (Bilston, United Kingdom). These fibers were cut, from the same batch, to a 20 mm mean length after a two-step reclaiming process. According to previous collaborations with UK researchers [20, 21], the two-step treatment consists of a pyrolysis treatment of 30 min at 500 °C under nitrogen followed by a second step of thermo-oxidation of 10 min at 500 °C under air to remove the char produced during pyrolysis. A third type of fiber was prepared by making the virgin fibers undergo a thermo-oxidative treatment similar to the char-removing treatment used by ELG, in order to eliminate the coating. Virgin fibers were heated up to 500 °C in an oven for 10 min under air. For clarity purposes, virgin fibers are hereafter noted as VF, commercial reclaimed fibers as RCF, and virgin fibers after thermal treatment as VFT.

2.2. CF/PA6 microdroplets sample preparation

In order to perform interfacial shear strength tests, samples composed of a microdroplet on a single carbon fiber are required. These samples were prepared using the following non-standard method (quite similar to the one employed by Ma et al. [22]): a single CF was fixed on one end to a plastic tab using a photocured resin. Then PA6 powder finely ground in liquid nitrogen was used to cover the free end of the CF using electrostatic interaction. Finally, the thermoplastic powder was melted using a copper wire to selectively heat up the free end of the CF to 230 °C. The microdroplets were then naturally formed by capillarity of the melted thermoplastic. An example of a droplet is shown in figure 1.

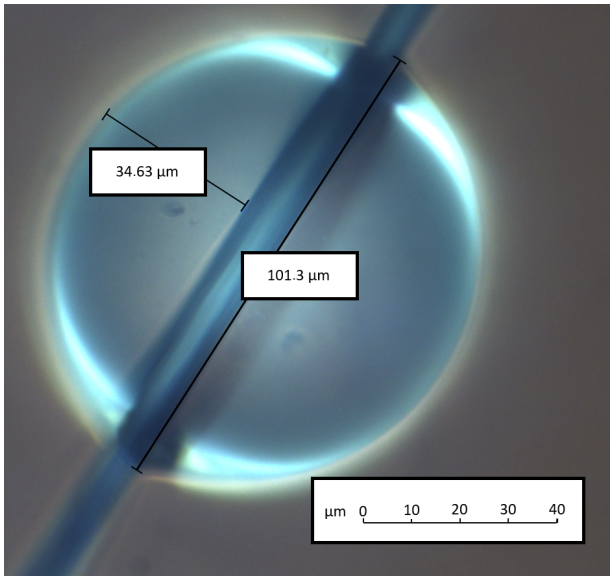

Figure 1: Microdroplet sample observed via optical microscopy

Embedded lengths were measured using an optical microscope equipped with a camera. To avoid fiber breakage during the IFSS tests, the microdroplets were selected so that the embedded length was less than 130 µm.

2.3. Characterization

2.3.1. Fibers tensile testing

Mechanical characterization of fibers was conducted using a LEX820 from Dia-Stron (Andover, UK). Prior to tensile testing, fibers transverse dimensions were measured using a FDAS770 Fiber Dimensional Analysis System from Dia-Stron. 200 projections were collected by rotating the fiber at each of the 20 locations along its axis in order to get the minimum and maximum diameters D_{min} and D_{max}. Assuming an elliptical shape for each cross-section, 20 cross-sectional areas were computed. The mean value of these cross-sectional areas was noted S_{mean}. From the force at break F, the tensile strength σ was calculated according equation (1):

$$\sigma = \frac{F}{S_{mean}} \tag{1}$$

Displacement values obtained during tensile testing were adjusted to account for the experimental set-up inherent compliance according to the ISO

11566:1996 standard. The compliance value used was 0.28 mm.N^{-1}. To ensure repeatability, 25 samples were tested for each fiber type with a nominal fiber length of 12 mm. Tensile moduli were determined by linear regression of the stress vs strain plots, in the elastic deformation domain between 0.05 % and 0.25 % deformation according to the ISO 11566:1996 standard.

2.3.2. X-ray Photoelectron Spectrometry

The apparatus used for elemental compositions and interfacial interactions analyses is an ESCALAB 250 photoelectron X-ray spectrometer (XPS) from Thermo Electron (Waltham, MA, USA). The excitation source was an Al Kα monochromatic source (1486.6 eV). The analyzed surface had a diameter of 500 µm. Spectra were recorded from at least three distinct locations on each sample, with a 1 $\times$ 1 mm^2 area of analysis. The analysis depth of the XPS probe is about 10 nm. The photoelectron spectra were calibrated in binding energy with respect to the energy of the C-C component of carbon C1s at 284.8 eV. The charge is compensated by a low energy electron beam (-2 eV). Several CF sections were randomly chosen from the three fiber types. The C1s, O1s, N1s and Si2p electron binding energy were referenced at 293.25 eV, 538.08 eV, 404.58 eV and 105.1 eV, respectively.

2.3.3. Scanning Electron Microscopy

The surface morphology of fibers was observed using a Quanta 200 FEG scanning electron microscope (SEM) from FEI Company (Hillsboro, OR, USA), operating at 4 kV.

2.3.4. Atomic Force Microscopy

A MFP-3D Infinity atomic force microscope (AFM) from Asylum Research (Santa Barbara, CA, USA) was used in tapping mode to assess the topography of fibers. From this topographic data, roughness values were computed. Single fibers were fixed to a glass slide for testing. A silicon probe (AC160TS-R3) with a resonant frequency of 300 kHz and a spring constant of 25 N/m was used. Scan rate was set to 1 Hz. Topography images of 3$\times$3 µm^2 with a resolution of 256 $\times$ 256 pixels were obtained. Three-dimensional topography of the fiber's surface was acquired using IGOR Pro 6.27 software.

To deduce roughness values from the scans, raw topography data was processed using Matlab (non-standard method) so that the global curvature of the fiber surface did not influence roughness evaluation. Each acquired

data point was defined by its height z, its abscissa x and its ordinate y. The shape of the fiber global surface as a distribution of heights $z(x, y)$ was interpolated in Matlab using a fourth-order polynomial function expressed as (2):

$$z_{interp} = \sum_{i,j=0}^{i+j\leq 4} a_{ij} x^i y^j \tag{2}$$

The a_{ij} coefficients were fitted, in the least squares sense, by minimizing the residual scalar ϵ which quantifies the distance between this interpolation surface and the measured topography z. ϵ being defined as (3):

$$\epsilon = \sum_{\substack{x_{min}\leq x\leq x_{max} \\ y_{min}\leq y\leq y_{max}}} (z(x, y) - z_{interp}(x, y))^2 \tag{3}$$

Then, subtracting the interpolated surface from the topography data led to the local deviations dz from the surface main shape (4):

$$dz(x, y) = z(x, y) - z_{interp}(x, y) \tag{4}$$

These deviations highlight the roughness and enable its evaluation according to a classical statistical descriptor such as the root mean square height Sq (ISO 25178-2:2021 standard) expressed as (5):

$$Sq = \sqrt{\frac{1}{A} \iint_A dz^2(x, y)\, dx\, dy} \tag{5}$$

Sq was the main value used to quantify the fibers surface roughness.

2.3.5. Contact angle measurements

Before contact angle determination, each fiber cross-section was individually measured with the Dia-Stron FDAS770 Fiber Dimensional Analysis System using the protocol outlined in the 2.3.1 section. Contact angle measurement of single fibers surface was executed with a Krüss K100 SF tensiometer at ambient temperature using the Wilhelmy method [23]. Test liquids used were n-hexane, water, diiodomethane and ethylene glycol. n-Hexane was used as a totally dispersive liquid, water was used for its high polarity and surface tension, diiodomethane was used for its weak polarity while not being

totally dispersive, and ethylene glycol was used for its good balance of polarity and dispersivity (corresponding surface energies are gathered in table 1).

Table 1: Surface energy polar and dispersive components for each test liquid

	γ_l^p [mN.m^{-1}]	γ_l^d [mN.m^{-1}]
n-Hexane	0	18.4
Water	51	21.8
Diiodomethane	2.3	48.5
Ethylene glycol	19	29

The vessel speed was set at 1 mm.min^{-1} for an immersion of 3 mm. Contact angles were determined using the Wilhelmy relationship (6):

$$F_c = P.\gamma_l.\cos\theta \tag{6}$$

With F_c being the capillary force measured by the tensiometer, P being the perimeter of the fiber, γ_l being the surface energy of the test liquid, and θ being the measured contact angle. Fiber cross-section was considered elliptical, and its perimeter was approximated using the Ramanujan approximation [24], described as (7):

$$P = 3(D_{min} + D_{max}) - \sqrt{(3D_{min} + D_{max})(D_{min} + 3D_{max})} \tag{7}$$

D_{min} and D_{max} are respectively the mean values of the minimum and maximum diameter, determined for each fiber type using the Dia-Stron FDAS770 Fiber Dimensional Analysis System. The buoyancy effect was neglected due to the very low volume of the fibers. Indeed, the induced force would be lower than the resolution of the device. The advancing and receding dynamic contact angles, as well as the static contact angle were acquired. Only the static contact angle was considered for the surface energies determination. Reported contact angles mean values for a given test liquid were obtained from an average over at least 7 contact angles. Surface energies of the fibers were deduced using the Owens-Wendt relation with a linear representation (8):

$$\frac{\gamma_l(1+\cos\theta)}{2\sqrt{\gamma_l^d}} = \sqrt{\gamma_s^p}\frac{\sqrt{\gamma_l^p}}{\sqrt{\gamma_l^d}} + \sqrt{\gamma_s^d} \tag{8}$$

Once components of test liquids and equilibrium contact angles are known, this equation enables the determination of the dispersive and polar components of the solid surface energy (γ_s^d and γ_s^p).

2.3.6. Microdroplet IFSS testing

Mechanical characterization of the fiber/matrix interfacial strength was conducted using the Dia-Stron LEX820 outlined in the 2.3.1 section, equipped with a microdroplet pull-out module and a 20 µm vise. Positions of the droplets on the fiber were measured using an optical microscope to ensure proper initial positioning of the droplet relative to the vise. The embedded fiber length was optically evaluated as well, in the perspective of the IFSS calculus.

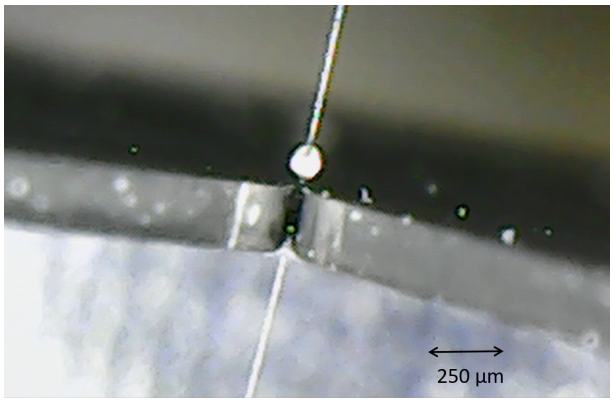

Figure 2: Microbond sample positioning relative to a 20 µm vise (image captured using an endoscopic microscope camera)

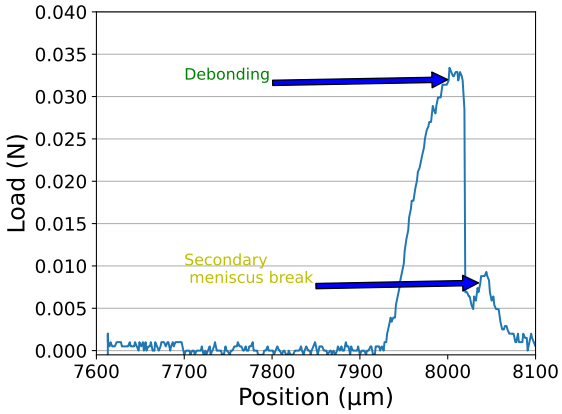

Figure 3: Load (N) as a function of displacement (µm) during a typical microbond test

Testing speed was set to 0.005 mm.s^{-1}. The droplet used for testing was positioned 500 µm away from the IFSS vise as illustrated in figure 2 and then pulled over 800 µm. The contact with the testing vise resulted in an increasing load. A typical microbond test plot is represented in figure 3. A first peak corresponding to the droplet debonding is visible, followed by a secondary peak induced by the fracture of the second meniscus of the droplet. The peak force value F, at which the droplet detaches from the fiber under the shear forces, was then used to deduce the IFSS value from the equation (9):

$$IFSS = \frac{F}{L.P} \tag{9}$$

L is the embedded length determined via optical microscopy, and P is the perimeter of the fiber approximated using the method described in 2.3.5.

3. Results and discussion

3.1. Fibers mechanical properties

The tensile strength values obtained with the method presented in 2.3.1 are presented as a boxplot in figure 4. As expected, a clear difference of about 15 % is observed between RCF and the two other fiber types. The diminution of tensile strength values is consistent with the mechanical performance claimed by the supplier and the literature [25, 26].

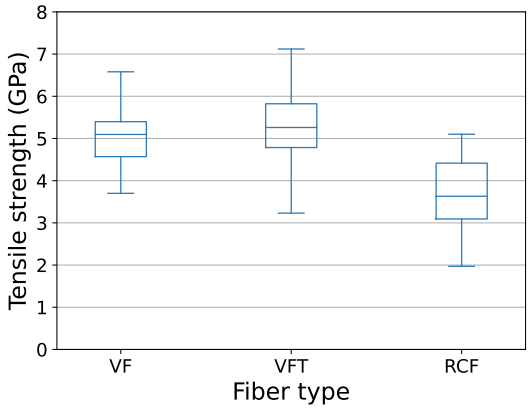

Figure 4: Ultimate tensile strength values for each fiber type

VFT and VF tensile strength values do not show a significant difference which suggests that the short (10 min) thermo-oxidative part of the recycling process is not detrimental to the strength of fibers. However, after the full recycling process (50 min total), RCF show a reduced tensile strength of about 15 % compared to VF. Prolonged exposure to high temperatures (above 500 °C), even under inert atmosphere, is correlated in the literature with a diminution of the fibers mass and diameter. It results in a higher concentration of fracture-inducing defects in a given volume [27]. This has a direct impact on the fiber strength, as highlighted by the tensile strength values obtained from RCF compared to VF.

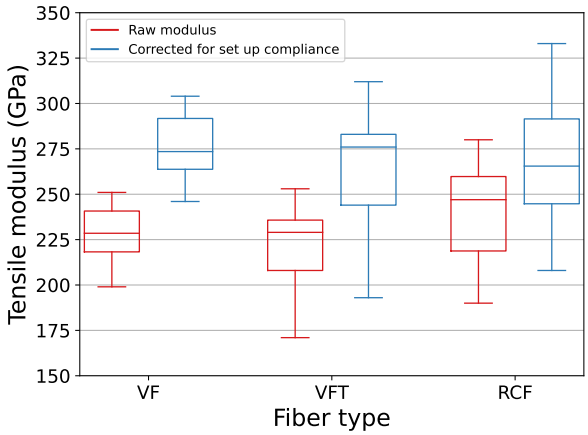

Figure 5: Tensile modulus values of each fiber type, calculated using raw displacement input and corrected for system compliance

On the other hand, tensile moduli do not appear to be significantly affected by the thermal treatment or recycling comparatively to VF, as seen in figure 5. This observation, combined to the tensile strength results, indicates that the recycling process has a negative effect on the fibers mechanical properties. This process is likely to extend the incidence of defects and thus to increase the probability of rupture for a given tensile stress, without significantly affecting the elastic properties of fibers.

3.2. Fibers surface chemical analysis

Full wide scan XPS spectrum (survey) of the three fiber types are displayed in figure 6 as a function of binding energy (BE). The individual peaks used to determine the prevalence of BE chemical functional groups by curve-fitting analysis are displayed in figure 7 for C1s and O1s.

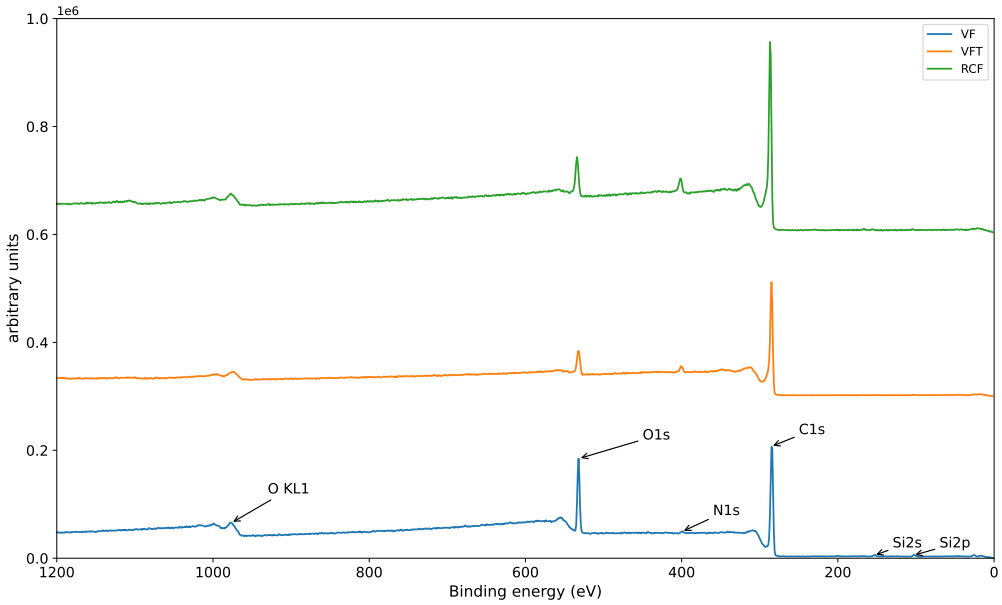

Figure 6: High-resolution wide scan XPS spectra of (a) VF, (b) VFT, and (c) RCF (VFT and RCF spectra were shifted vertically for clarity purposes)

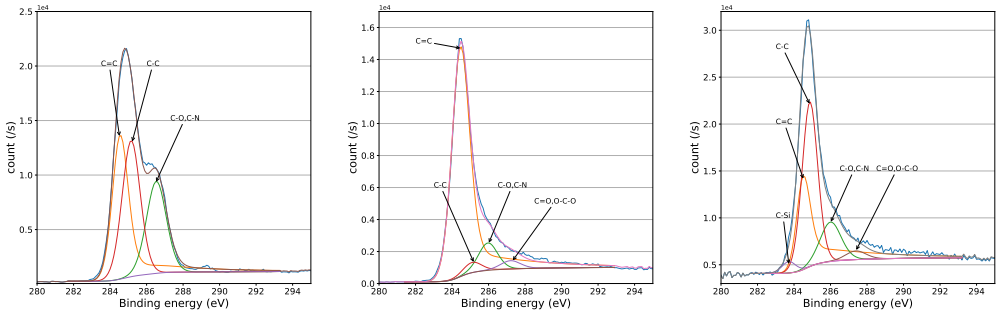

(a) (b) (c)

(d) (e) (f)

Figure 7: C1s scan of (a) VF, (b) VFT, (c) RCF, and O1s scan of (d) VF, (e) VFT, (f) RCF

Table 2: Surface elemental and chemical composition for each fiber type

	VF		VFT		RCF	
	Peak BE [eV]	Atomic fraction	Peak BE [eV]	Atomic fraction	Peak BE [eV]	Atomic fraction
C1s	284.8	85.8 %	284.9	78.6 %	284.8	87.7 %
O1s	532.1	8.3 %	533.1	19.2 %	532.0	8.8 %
O/C ratio	-	0.10	-	0.24	-	0.10

According to the repeatability tests performed in this study (4 tests per sample) and the literature, the uncertainty for the atomic percentages obtained is 0.5 % (one standard deviation) [28, 29]. These values along with O/C ratios for VF (sized fibers), VFT (de-sized fibers due to thermal treatment) and RCF (recycled fibers) are found in Table 2. VF exhibit a 0.24 O/C ratio whereas those of RCF and VFT are 60 % lower, 0.10 for both materials. Previous studies showed that the O/C ratio is a reliable indicator of the chemical bonding ability of the fiber to the targeted thermoplastic matrix [19, 30, 31, 32]. This is in accordance with the higher O/C ratio of VF resulting from the presence of sizing.

Table 3: C-OH atomic percentages for each fiber type

	C-OH atomic fraction [%]
VF	20.3
VFT	8.0
RCF	12.3

A detailed analysis of the different peaks indicates that, although the O/C ratio of VFT and RCF are similar, their chemical bonding properties are different. This is due to different functional groups proportions. The peak corresponding to C-OH bonds (286 eV) is largely inferior for RCF and VFT compared to VF (atomic percentage values are gathered in table 3). It suggests that the oxidation state of their surface is further diminished after treatment. This reduction in the higher oxidation state groups can be considered as a passivation of the surface after thermal treatment. However, the reduction in C-OH bonds is less pronounced in RCF, which may be related to the presence of polymer residues. Hence, RCF maintain a slightly higher

oxidation state after treatment and thus more functional groups positively associated to fiber/matrix chemical bonding.

3.3. Fibers surface morphology

3.3.1. Scanning Electron Microscopy

SEM images of the different fiber types are displayed in figure 8. A clear difference in the textures of the fiber surfaces is observable: VFT present a smooth surface, RCF have portions of smooth surfaces and chunks of residual polymer, while VF smooth surface is covered with darker spots like blisters on a paintwork. This observation is attributed to the heteogeneous distribution of the sizing over CF surface. Overall, the level of detail of these scans gives a good qualitative understanding of the different morphologies, but to further evaluate these differences and obtain a quantitative comparison, atomic force microscopy is required.

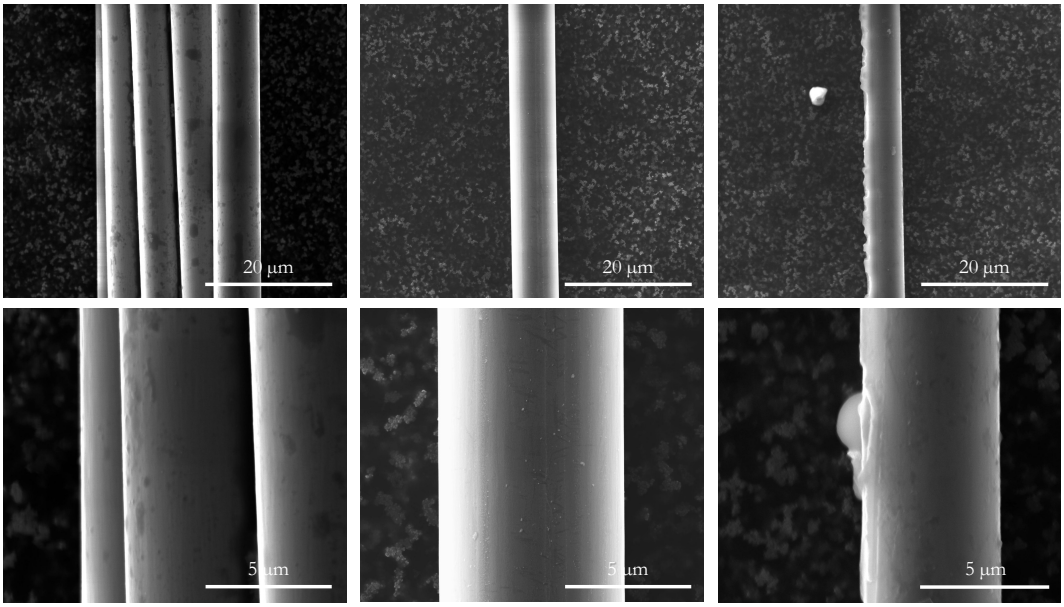

Figure 8: SEM scan of a) bundle of VF, b) VFT, c) RCF

3.3.2. Atomic Force Microscopy

AFM scans of VF and VFT, as well as RCF with and without polymer residues are displayed in figure 9. RCF scans were performed in different

regions from the same individual fiber to highlight the heterogeneity of the RCF surface morphology.

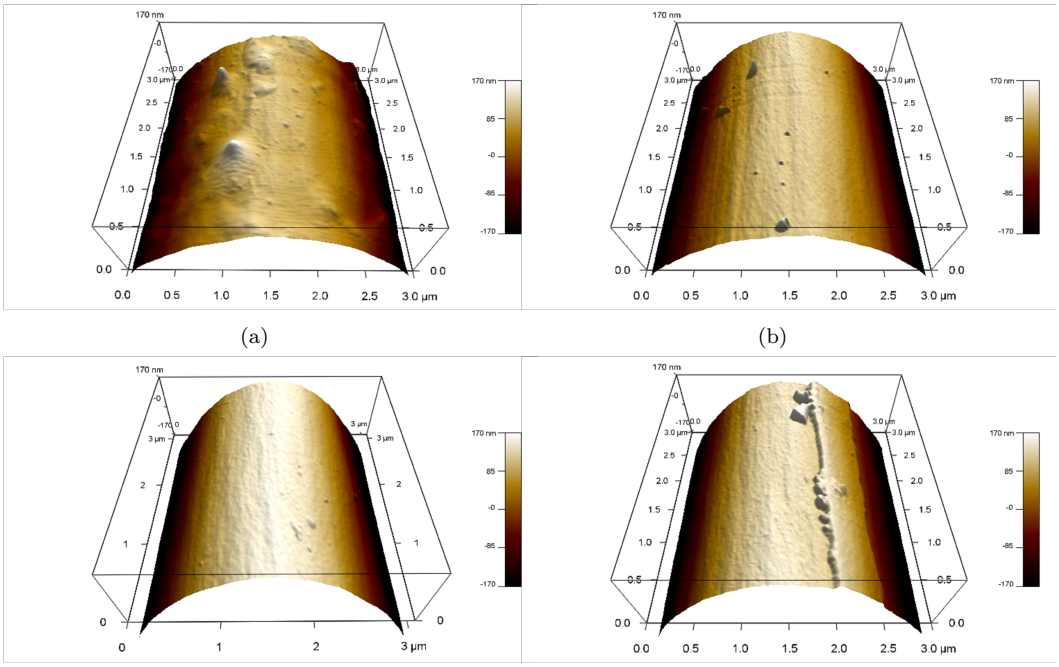

Figure 9: Topography of 3×3 µm^2 surfaces of (a) VF, (b) VFT, (c) smooth RCF, (d) RCF

The reconstructed images confirm SEM observations. RCF and VFT have very similar textures except parts of the RCF that still present polymeric residues. The VF surface looks more heterogeneous, the texture resulting from sizing being very distinct from the smooth fiber regions observable on the other two samples.

Table 4: Roughness measurements for each fiber type

	Sq [nm]	Highest peak [nm]	Deepest pit [nm]
VF	23.0	154.4	-53.9
VFT	5.6	43.0	-26.8
RCF (smooth)	3.4	27.4	-13.1
RCF	9.3	45.3	-31.9

The roughness data are presented in table 4. VF surface presents the highest roughness out of the three fiber types. Besides, VFT and regions without polymer residue of RCF present similar roughness values. These results suggest that VF has an advantage in fiber/matrix cohesion not only from better adhesion through chemical bonding but also better cohesion from mechanical interlocking due to higher roughness.

3.4. Fiber surfaces wettability

The linear representation of the Owens-Wendt relationship for each fiber type is presented in figure 10 and the resulting surface energies values gathered in table 5 and graphically represented in figure 11.

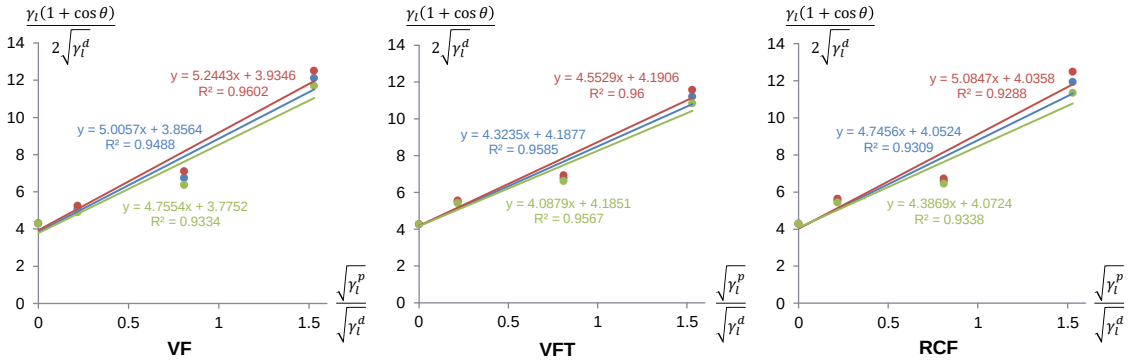

Figure 10: Surface energies, determined with the Owens-Wendt equation, for each fiber type

Table 5: Surface energy polar and dispersive components, as well as total energy, for each fiber type

	γ_s^p [mN.m^{-1}]	γ_s^d [mN.m^{-1}]	γ_s [mN.m^{-1}]
VF	25.1 ± 2.5	14.9 ± 3.5	39.9 ± 6.0
VFT	18.7 ± 2.0	17.5 ± 0.9	36.2 ± 2.9
RCF	22.5 ± 3.3	16.4 ± 2.0	38.9 ± 5.3

The ratios of polar component over total energy are 0.63 ± 0.028 for VF, 0.52 ± 0.014 for VFT, and 0.58 ± 0.006 for RCF. In literature, the total surface energy and the ratio of polar component over said total energy seem to be the main predictors of the cohesion between fibers and polymer matrix

(i.e., strength of composites parts and IFSS values) [33, 34]. Total surface energies does not show significant differences between the three fiber types. The polar component over total energy ratios however show that RCF has a better potential for adhesion than VFT with a significantly higher ratio. This potential for adhesion to the PA6 matrix is still not on par with VF which exhibits the higher ratio by a large margin.

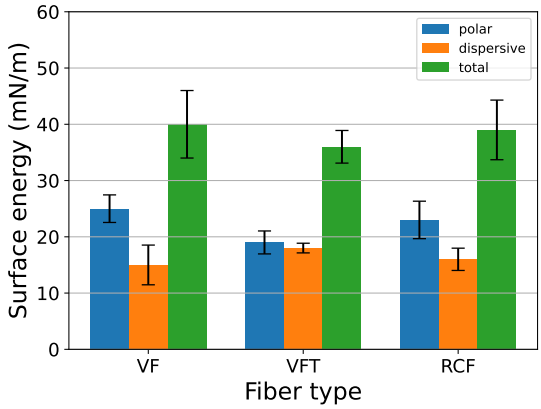

Figure 11: Surface energies for each fiber type

Based on average values of surface energies and polar/total surface energy ratio, RCF could exhibit a better potential for adhesion to polyamide 6 than VFT. This could be due to the residual polymer not eliminated by the recycling process allowing for better chemical bonding. However, in order to confirm the hypothesis of a better adhesion with matrix, PA6 surface properties should be determined.

3.5. Interfacial shear strength characterization

The interfacial shear strength values obtained from microdroplets pull-out tests are shown in figure 12. Interfacial shear strength between PA6 and VFT or RCF is about 35 % lower than with VF. This confirms that, in the case of thermoplastics and short carbon fiber composites, sizing has a pronounced beneficial effect on bonding strength [35]. Furthermore, it is in accordance with the higher O/C ratio determined via chemical analysis of the fibers surface. Similarly, VFT and RCF have identical O/C ratios and similar interfacial strengths.

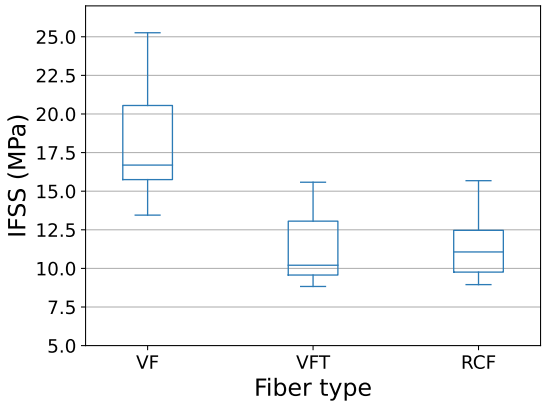

Figure 12: IFSS mean values for each fiber type

These results suggest that cohesion between fibers and matrix is most likely affected both by physico-chemical properties (adhesion) and roughness (mechanical interlocking) of fibers surface. However, manipulating surface roughness of fibers via thermal treatments does not appear to be a reliable way to increase cohesion strength in composites. This is partly due to the decrease in fiber diameter and the associated increased probability of rupture-initiating defects. Consequently, modifying the chemistry of RCF surface via surface treatments to increase the O/C ratio seems to be the most promising approach to reuse RCF in high performance applications.

4. Conclusions

VF, VFT and RCF mechanical and surface properties were evaluated and compared. Results showed that the reclaiming process has a limited impact on the mechanical properties of fibers with a decrease of 15 % of their tensile strength compared to virgin and de-sized fibers, whereas their tensile modulus is unaffected. Consequently, the intrinsic mechanical properties of RCF are not a major drawback for reuse, unlike their surface properties and adhesion capacities. The ratio of RCF polar component over their total surface energy is 8 % lower than that of VF, and similarly the ratio of VFT is 17 % lower than that of VF. Even though the measurements were performed at ambient temperatures, these values indicate a significant reduction of the adhesion with the matrix during processing when fibers and matrix

are mixed together at higher temperatures. This finding is in accordance with the IFSS tests for which IFSS values of RCF and VFT are reduced by 35 % compared to VF. Wettability measurements and chemical state evaluation of RCF surfaces indicate that the presence of residual polymer has a positive effect on RCF/matrix adhesion capability compared to VFT. On the contrary, VFT surfaces are smooth, and the thermal treatment induces a substantial passivation of the surface which is characterized by a diminution of the proportion of higher oxidation state functional groups. In addition, the higher surface energy values and higher degree of surface oxidation observed for VF do correlate with a higher interfacial strength compared to the other fiber types. However, VFT and RCF have similar interfacial strength. A possible explanation for this discrepancy would be that the difference in adhesion capability between RCF and VFT is too small to create a significant difference in interfacial strength. In that case, the most promising approach to obtain highly reusable RCF would be to functionalize their surface to create a surface chemical state as close as possible to that of VF, resulting in higher interfacial strength. In further research, chemical treatments of RCF surface will be considered to enhance their chemical bonding to matrix. Recent studies on re-sizing of scraps and outdated pieces of uncured carbon fiber prepregs from the aeronautic sector with silane based coupling agents showed mixed results going from a diminution of 10 % of the IFSS to an augmentation of 27 % depending on the coupling agent used [36, 37]. In a similar fashion cold plasma treatment used on scrap de-sized fibers has been found to improve IFSS by up to 30 % depending on the type of plasma, exposure time and other process related parameters [12, 18]. Both are interesting option but will need a comparative analysis in the case of pyrolysis recycled carbon fiber to assess their usefullnes in restoring the surface properties of thermally treated fibers.

CRediT authorship contribution statement

Louis Jeantet: Conceptualization, Methodology, Investigation, Writing - Original Draft, Visualization. **Arnaud Regazzi:** Conceptualization, Methodology, Validation, Writing - Review & Editing, Supervision, Project administration. **Didier Perrin:** Methodology, Validation, Investigation, Writing - Review & Editing. **Monica Francesca Pucci:** Methodology, Validation, Investigation, Writing - Review & Editing. **Stéphane Corn:** Methodology, Validation, Formal analysis, Writing - Review & Editing. **Jean-**

Christophe Quantin: Methodology, Validation, Writing - Review & Editing. **Patrick Ienny:** Conceptualization, Methodology, Validation, Writing - Review & Editing, Supervision, Funding acquisition.

Declaration of Competing Interest

The authors declare that they have no known competing financial interests or personal relationships that could have appeared to influence the work reported in this paper.

Data availability

Data will be made available on request.

Acknowledgments

Primary funding for this research was provided by Segula Technologies. The authors would like to thank Benjamin Gallard and Jean-Claude Roux for sample preparation as well as valuable scientific insights on the topic of composite production and characterization. The authors also acknowledge Valérie Flaud (Institut Charles Gerhardt Montpellier, Montpellier, France) for her contribution in conducting XPS experiments and valuable assistance in analyzing XPS data.

References

[1] Darli Rodrigues Vieira, Raimundo Kennedy Vieira, and Milena Chang Chain. Strategy and management for the recycling of carbon fiber-reinforced polymers (cfrps) in the aircraft industry: a critical review. *International Journal of Sustainable Development & World Ecology*, 24(3):214–223, 2017.

[2] Tushar Kanti Das, Prosenjit Ghosh, and Narayan Ch Das. Preparation, development, outcomes, and application versatility of carbon fiber-based polymer composites: a review. *Advanced Composites and Hybrid Materials*, pages 1–20, 2019.

[3] David T Burn. *Long discontinuous carbon fibre/polypropylene composites for high volume automotive applications*. PhD thesis, University of Nottingham, 2016.

[4] Jin Zhang, Gang Lin, Uday Vaidya, and Hao Wang. Past, present and future prospective of global carbon fibre composite developments and applications. *Composites Part B: Engineering*, page 110463, 2022.

[5] Fanran Meng, Jon McKechnie, Thomas Turner, Kok H Wong, and Stephen J Pickering. Environmental aspects of use of recycled carbon fiber composites in automotive applications. *Environmental science & technology*, 51(21):12727–12736, 2017.

[6] Fanran Meng, Elsa A Olivetti, Youyang Zhao, Jiyoun C Chang, Stephen J Pickering, and Jon McKechnie. Comparing life cycle energy and global warming potential of carbon fiber composite recycling technologies and waste management options. *ACS Sustainable Chemistry & Engineering*, 6(8):9854–9865, 2018.

[7] Sudheer Kumar and Sukhila Krishnan. Recycling of carbon fiber with epoxy composites by chemical recycling for future perspective: a review. *Chemical Papers*, 74:3785–3807, 2020.

[8] Liang Yue, Mehrad Amirkhosravi, Xuehui Gong, Thomas G Gray, and Ica Manas-Zloczower. Recycling epoxy by vitrimerization: Influence of an initial thermoset chemical structure. *ACS Sustainable Chemistry & Engineering*, 8(33):12706–12712, 2020.

[9] Xiang Li, Ruibin Bai, and Jon McKechnie. Environmental and financial performance of mechanical recycling of carbon fibre reinforced polymers and comparison with conventional disposal routes. *Journal of Cleaner Production*, 127:451–460, 2016.

[10] YF Khalil. Sustainability assessment of solvolysis using supercritical fluids for carbon fiber reinforced polymers waste management. *Sustainable Production and Consumption*, 17:74–84, 2019.

[11] Félix A López, Olga Rodríguez, Francisco José Alguacil, Irene García-Díaz, Teresa A Centeno, José Luis García-Fierro, and Carlos González. Recovery of carbon fibres by the thermolysis and gasification of waste prepreg. *Journal of analytical and applied pyrolysis*, 104:675–683, 2013.

[12] Song Hee Han, Hyun Ju Oh, and Seong Su Kim. Evaluation of fiber surface treatment on the interfacial behavior of carbon fiber-reinforced

polypropylene composites. *Composites Part B: Engineering*, 60:98–105, 2014.

[13] Febo Severini, Leonardo Formaro, Mario Pegoraro, and Luca Posca. Chemical modification of carbon fiber surfaces. *Carbon*, 40(5):735–741, 2002.

[14] Gregory J Ehlert, Yirong Lin, and Henry A Sodano. Carboxyl functionalization of carbon fibers through a grafting reaction that preserves fiber tensile strength. *Carbon*, 49(13):4246–4255, 2011.

[15] Zhangping Wen, Cheng Xu, Xin Qian, Yonggang Zhang, Xuefei Wang, Shulin Song, Mingzhi Dai, and Cheng Zhang. A two-step carbon fiber surface treatment and its effect on the interfacial properties of cf/ep composites: The electrochemical oxidation followed by grafting of silane coupling agent. *Applied Surface Science*, 486:546–554, 2019.

[16] Xin Qian, Xuefei Wang, Qin Ouyang, Yousi Chen, and Qing Yan. Effect of ammonium-salt solutions on the surface properties of carbon fibers in electrochemical anodic oxidation. *Applied Surface Science*, 259:238–244, 2012.

[17] Chengcheng Sun, Junying Min, Jianping Lin, and Hailang Wan. Effect of atmospheric pressure plasma treatment on adhesive bonding of carbon fiber reinforced polymer. *Polymers*, 11(1):139, 2019.

[18] Hooseok Lee, Haowen Wei, and Jun Takahashi. The influence of plasma in various atmospheres on the adhesion properties of recycled carbon fiber. *Macromolecular Research*, 23(11):1026–1033, 2015.

[19] Christoph Unterweger, Jiri Duchoslav, David Stifter, and Christian Fuerst. Surface properties of carbon fibers: Impact on the mechanical performance of short fiber reinforced polypropylene composites. *20th International Conference on Composite Materials*, 07 2015.

[20] Mark Holmes. Recycled carbon fiber composites become a reality. *Reinforced Plastics*, 62(3):148–153, 2018.

[21] MH Akonda, CA Lawrence, and BM Weager. Recycled carbon fibre-reinforced polypropylene thermoplastic composites. *Composites Part A: Applied Science and Manufacturing*, 43(1):79–86, 2012.

[22] Yunyun Ma, Chun Yan, Haibing Xu, Dong Liu, Pengcheng Shi, Yingdan Zhu, and Junlong Liu. Enhanced interfacial properties of carbon fiber reinforced polyamide 6 composites by grafting graphene oxide onto fiber surface. *Applied Surface Science*, 452:286–298, 2018.

[23] Claudio Della Volpe and Stefano Siboni. The wilhelmy method: a critical and practical review. *Surface Innovations*, 6(3):120–132, 2018.

[24] Mark B Villarino. Ramanujan's inverse elliptic arc approximation. *The Ramanujan Journal*, 34(2):157–161, 2014.

[25] Di He, Vi Kie Soo, Filip Stojcevski, Wojciech Lipiński, Luke C Henderson, Paul Compston, and Matthew Doolan. The effect of sizing and surface oxidation on the surface properties and tensile behaviour of recycled carbon fibre: An end-of-life perspective. *Composites Part A: Applied Science and Manufacturing*, 138:106072, 2020.

[26] Jin-Soo Jeong, Kwan-Woo Kim, Kay-Hyeok An, and Byung-Joo Kim. Fast recovery process of carbon fibers from waste carbon fibers-reinforced thermoset plastics. *Journal of environmental management*, 247:816–821, 2019.

[27] TR Abdou, AB Botelho Junior, DCR Espinosa, and JAS Tenório. Recycling of polymeric composites from industrial waste by pyrolysis: Deep evaluation for carbon fibers reuse. *Waste Management*, 120:1–9, 2021.

[28] CJ Powell and Mo P Seah. Precision, accuracy, and uncertainty in quantitative surface analyses by auger-electron spectroscopy and x-ray photoelectron spectroscopy. *Journal of Vacuum Science & Technology A: Vacuum, Surfaces, and Films*, 8(2):735–763, 1990.

[29] K Harrison and LB Hazell. The determination of uncertainties in quantitative xps/aes and its impact on data acquisition strategy. *Surface and interface analysis*, 18(5):368–376, 1992.

[30] Tao Zhang, Yueqing Zhao, Hongfu Li, and Boming Zhang. Effect of polyurethane sizing on carbon fibers surface and interfacial adhesion of fiber/polyamide 6 composites. *Journal of Applied Polymer Science*, 135(16):46111, 2018.

[31] Chen Hui, Cai Qingyu, Wu Jing, Xia Xiaohong, Liu Hongbo, and Luo Zhanjun. Interfacial enhancement of carbon fiber/nylon 12 composites by grafting nylon 6 to the surface of carbon fiber. *Applied Surface Science*, 441:538–545, 2018.

[32] J Li and CL Cai. The carbon fiber surface treatment and addition of pa6 on tensile properties of abs composites. *Current Applied Physics*, 11(1):50–54, 2011.

[33] William Garat, Monica Francesca Pucci, Romain Léger, Quentin Govignon, Florentin Berthet, Didier Perrin, Patrick Ienny, and Pierre-Jacques Liotier. Surface energy determination of fibres for liquid composite moulding processes: method to estimate equilibrium contact angles from static and quasi-static data. *Colloids and Surfaces A: Physicochemical and Engineering Aspects*, 611:125787, 2021.

[34] Xiang Chen, Haibing Xu, Dong Liu, Chun Yan, Youqiang Yao, and Yingdan Zhu. Effect of hybrid polysphosphazene coating treatment on carbon fibers on the interfacial properties of cf/pa6 composites. *Journal of Applied Polymer Science*, 137(37):49577, 2020.

[35] RL Zhang, YD Huang, D Su, L Liu, and YR Tang. Influence of sizing molecular weight on the properties of carbon fibers and its composites. *Materials & Design*, 34:649–654, 2012.

[36] Hyunkyung Lee, Min-su Kim, Gyungha Kim, and Daeup Kim. Effect of the chemical properties of silane coupling agents on interfacial bonding strength with thermoplastics in the resizing of recycled carbon fibers. 2023.

[37] Sarianna Palola, Pekka Laurikainen, Sonia García-Arrieta, Egoitz Goikuria Astorkia, and Essi Sarlin. Towards sustainable composite manufacturing with recycled carbon fiber reinforced thermoplastic composites. *Polymers*, 14(6):1098, 2022.